Numerical studies of backscattering enhancement of electromagnetic waves from two-dimensional random rough surfaces with the forward–backward/novel spectral acceleration method

Danai Torrungrueng and Joel T. Johnson

ElectroScience Laboratory, Department of Electrical Engineering, The Ohio State University, 1320 Kinnear Road, Columbus, Ohio 43212

Received November 30, 2000; revised manuscript received March 5, 2001; accepted March 15, 2001

The forward–backward method with a novel spectral acceleration algorithm (FB/NSA) has been shown to be a highly efficient $\mathcal{O}(N_{\text{tot}})$ iterative method of moments, where N_{tot} is the total number of unknowns to be solved, for the computation of electromagnetic (EM) wave scattering from both one-dimensional and two-dimensional (2-D) rough surfaces. The efficiency of the method makes studies of backscattering enhancement from moderately rough impedance surfaces at large incident angles tractable. Variations in the characteristics of backscattering enhancement with incident angle, surface impedance, polarization, and surface statistics are investigated by use of the 2-D FB/NSA method combined with parallel computing techniques. The surfaces considered are Gaussian random processes with an isotropic Gaussian spectrum and root-mean-square surface heights and slopes ranging from 0.5λ to λ and from 0.5 to 1.0, respectively, where λ is the EM wavelength in free space. Incident angles ranging from normal incidence up to 70° are considered in this study. It is found that backscattering enhancement depends strongly on all parameters of interest.

OCIS codes: 290.1350, 290.5880, 290.4210.

1. INTRODUCTION

One of the most interesting phenomena associated with rough-surface scattering is the backscattering enhancement effect.[1,2] This phenomenon is associated with the appearance of a well-defined peak in the backscattering direction of the intensity of the incoherently scattered component of the electromagnetic (EM) field. Enhanced backscattering has been observed experimentally[3–6] from several rough-surface types. One such type involves surfaces with relatively large slopes for which predictions of the standard Kirchhoff approximation and of the small perturbation method are inaccurate because of the small slope limitations of these approximate theories. Although other approximate theories such as higher-order Kirchhoff approximation,[7] integral equation,[8] and full-wave[9] theories have been developed to explain the backscattering enhancement phenomenon, they remain restricted in their domains of validity. The limitations of the approximate analytical methods for large-slope surfaces and more-powerful modern computers have increased interest in numerical techniques based on Monte Carlo simulations, which have been successful in predicting backscattering enhancement in previous studies.[10–15] The most commonly applied technique is the surface integral equation and its solution by the method of moments, which determines fields scattered at a single frequency through inversion of a matrix equation.[16] Most methods solve this matrix equation iteratively with a sequence of matrix–vector multiply operations, reducing the operation count from $\mathcal{O}(N_{\text{tot}}^3)$ for a direct matrix inversion to $\mathcal{O}(N_{\text{tot}}^2)$ per iteration, where N_{tot} is the total number of unknowns to be solved. Efficiency is then improved by reducing the number of iterations required in the iterative solver or by reducing the operation count needed to perform a matrix-vector multiply.

One way to reduce computational requirements is to model surfaces as being rough in one direction only, i.e., as a two-dimensional (2-D) scattering problem. Whereas one-dimensional (1-D) surface models may be adequate for co-polarized scattering, a 2-D surface model that corresponds to a full three-dimensional computation is required for predicting cross-polarized scattering. Since backscattering enhancement, like cross-polarized scattering, is related to multiple-scattering effects, cross-polarized fields should illustrate the backscattering enhancement effect more clearly than co-polarized fields. However, 2-D surfaces greatly increase computational requirements since the surface profile and the surface fields must be discretized in both dimensions. Thus efficient numerical methods are indispensable tools for studying backscattering enhancement numerically.

Several previous studies of backscattering enhancement from very rough surfaces with relatively large slopes have been performed with both 1-D and 2-D surfaces. However, to our knowledge, numerical results based on Monte Carlo simulations for 2-D surfaces have not been reported for incident angles larger than 45°. Prediction of backscattering enhancement at large inci-

dent angles is quite challenging for analytical models because of the nonlocal interactions and increased shadowing effects involved. The absence of Monte Carlo results for this case is due to the computing limitation of previous studies, caused in part by the unavailability of efficient numerical techniques. The novel spectral acceleration (NSA) algorithm with the forward–backward (FB) method is a recently developed technique that has been shown to be a highly efficient $[\mathcal{O}(N_{\text{tot}})]$ iterative method for both 1-D and 2-D surfaces.[17–22] Because the NSA algorithm is still highly efficient for moderately rough large-scale surfaces and its memory storage requirement is very low compared with those of other fast techniques, numerical studies of backscattering enhancement from 2-D moderately rough surfaces at large incident angles are feasible. A previous paper[19] has illustrated that numerical results of the 2-D FB–NSA method are in good agreement with experimental data obtained from the University of Washington.[11]

In this paper, variations in the characteristics of backscattering enhancement with incident angle, surface material, polarization, and surface statistics are investigated with the 2-D FB–NSA method.[19,21,22] Incident angles ranging from normal incidence up to 70° are considered in this study. Because larger surface lengths are required primarily in the along-range direction and not in the cross-range direction as the incident angle increases, a rectangular surface size is used to reduce the number of unknowns. However, the surface size must be chosen appropriately such that numerical results obtained from Monte Carlo simulations are accurate. In this study, a rectangular surface size of 128λ by 16λ sampled with eight unknowns per wavelength, resulting in 262,144 unknowns, is employed, where λ is the EM wavelength in free space. This surface size is chosen such that numerical results are reasonably accurate for incident angles up to 70°, as we discuss in Section 2. For consistency, we employ the same surface size for all incident angles of interest in order to have the same surface realizations, even though smaller surface sizes could be sufficient for smaller incident angles. Computational resources available for the study allow 150 surface realizations to be included in the Monte Carlo simulation; the surfaces studied are Gaussian random processes with an isotropic Gaussian spectrum ($0.5\lambda \leqslant h \leqslant \lambda$ and $0.5 \leqslant \sigma_s \leqslant 1.0$, where h and σ_s are the rms surface height and the rms surface slope, respectively).

Although the FB–NSA method is a highly efficient iterative technique, the numerical problem of interest is still extremely computationally intensive. Parallel computing techniques are incorporated into the FB–NSA method so that the Monte Carlo simulations can be performed in parallel. Results were obtained with CRAY T3E and IBM Power2 Super Chip (P2SC) Symmetric Multiprocessing (SMP) (P2SC/SMP) systems. The CRAY T3E computer at the Ohio Supercomputing Center has a total of 136 processing elements, where each processing element includes a 300-MHz DEC 21164 CPU with 600 Mflops and 16 Mwords (128 Mbytes) of memory (see more details at http://www.osc.edu/). The IBM P2SC/SMP at the Maui High Performance Computing Center offers 224 P2SC batch nodes and two interactive SMP eight-processor nodes (see more details at http://www.mhpcc.edu/). The parallel algorithm developed simply runs distinct surface realizations in the Monte Carlo simulations on separate computing nodes and uses the message-passing interface (MPI) for task and processor controls.

This paper is organized as follows: A description of the problem is presented in Section 2, and Section 3 presents several numerical results of backscattering enhancement studies, including detailed discussions. A summary and conclusions can be found in Section 4. An $\exp(-i\omega t)$ time-harmonic convention is assumed and suppressed throughout this paper, and the propagation constant is defined as $k = \omega\sqrt{\mu\epsilon}$, where ω is the radian frequency and ϵ and μ are the permittivity and the permeability, respectively, of free space.

2. PROBLEM DESCRIPTION

Consider a 2-D rough-surface profile S illuminated by an incident field $\mathbf{E}^i(x, y, z)$ centered at the origin and propagating in direction $\hat{k}_i = \hat{x}\sin\theta_i\cos\phi_i + \hat{y}\sin\theta_i\sin\phi_i - \hat{z}\cos\theta_i$, as shown in Fig. 1, where θ_i and ϕ_i refer to the incident polar and azimuthal angles, respectively. Finite 2-D surface profiles with specified statistics are generated with a Fourier-transform technique.[6] The surface height function $z = f(x, y)$ has zero mean. The incident field $\mathbf{E}^i(x, y, z)$ is tapered with a Gaussian beam amplitude pattern confining the illuminated rough surface to the rectangular surface area $D_x \times D_y$ so that surface edges do not contribute strongly to the scattered fields. The tapered incident field is discussed in detail in Refs. 11, 22, and 23.

Surfaces considered are Gaussian random processes with an isotropic Gaussian spectrum given by

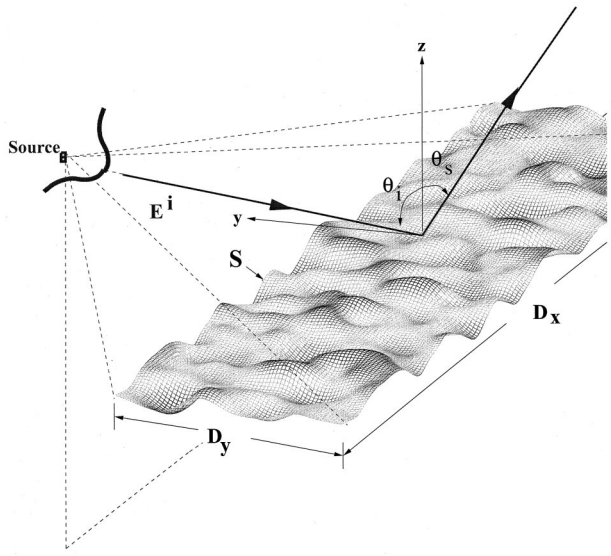

Fig. 1. 2-D rough-surface profile S illuminated by a tapered incident field $\mathbf{E}^i(x, y, z)$ centered at the origin and propagating in direction $\hat{k}_i = \hat{x}\sin\theta_i\cos\phi_i + \hat{y}\sin\theta_i\sin\phi_i - \hat{z}\cos\theta_i$.

$$W(k_x, k_y) = \frac{l^2 h^2}{4\pi} \exp\left[-\frac{1}{4}(k_x^2 + k_y^2) l^2 \right], \quad (1)$$

where $W(k_x, k_y)$ represents the spectrum amplitude, l is the surface correlation length, and k_x and k_y are the spatial frequencies in the x and the y directions, respectively. Rms surface slopes in the x and y directions, denoted $\sigma_{s,x}$ and $\sigma_{s,y}$, respectively, are identical for the isotropic Gaussian spectrum and are equal to $\sigma_s = \sqrt{2}h/l$. The total rms surface slope $\sigma_{s,\mathrm{tot}}$ is thus $\sqrt{2}\sigma_s$. In this study, three isotropic Gaussian spectra with a fixed surface correlation length $l = \sqrt{2}\lambda$ and $h/\lambda = \sigma_s = 0.5$, 0.707, and 1.0 are considered. As was pointed out in Ref. 1, rough surfaces that correspond to these parameters should exhibit backscattering enhancement. Surface materials considered in this study are perfect electric conductor (PEC) surfaces and surfaces that satisfy a local impedance boundary condition[24,25] IBC (neglecting surface curvature effects) with $\epsilon_{r1} = 38.0 + i40.0$ and $10.0 + i10.0$, where ϵ_{r1} is the relative permittivity of the nonmagnetic region below the surface profile. Tests of the IBC approximation were performed by comparing Monte Carlo simulations for impedance surfaces with results obtained from the small-perturbation method for small-height 1-D dielectric surfaces up to incident angle 85°.[22] In addition, Monte Carlo results obtained from 1-D impedance surfaces and 1-D dielectric surfaces for the roughest case ($h/\lambda = \sigma_s = 1.0$) and for all incident angles of interest ($0° \leqslant \theta_i \leqslant 70°$) are in good agreement.

To study polarization effects on backscattering enhancement, both co-polarization (HH and VV) and cross polarization (VH and HV) are considered, where H and V stand for horizontal and vertical polarizations, respectively. Previous studies have shown that cross polarization exhibits backscattering enhancement more clearly than does co-polarization because of the absence of the first-order scattering.[12,13] Incident angles ranging from normal incidence to 70° are considered, and the taper parameter g' employed in generating the incident field is chosen to be equal to 6.0.[22] With this value of g' and surface size 128λ by 16λ averaged with 150 surface realizations, numerical results are in good agreement at 70° with those from surface size 128λ by 32λ.

Use of the 2-D FB–NSA method requires a choice of several parameters that depend on the surface statistics.[19] Since the method is based on a spectral representation of the free-space scalar Green's function $g(\mathbf{r}, \mathbf{r}')$, numerical studies of the spectral domain representation of $g(\mathbf{r}, \mathbf{r}')$ can be used to determined these parameters for the three surface statistics of interest. Using the definitions of Ref. 19, we have found that

- For $h/\lambda = \sigma_s = 0.5$

  $L_x = 3.5\lambda$, $\gamma = 0.08\,\mathrm{rad}$, $a_{\max} = 1.0$, $k_{z,\mathrm{tail}} = 0.24k$, $k_{y,\mathrm{tail}} = 0.24\,\mathrm{Re}[\kappa]$, $C_z = 8.0$, $C_y = 14.0$.

- For $h/\lambda = \sigma_s = 0.707$

  $L_x = 4.0\lambda$, $\gamma = 0.08\,\mathrm{rad}$, $a_{\max} = 2.0$, $k_{z,\mathrm{tail}} = 0.2k$, $k_{y,\mathrm{tail}} = 0.24\,\mathrm{Re}[\kappa]$, $C_z = 11.0$, $C_y = 14.0$.

- For $h/\lambda = \sigma_s = 1.0$

  $L_x = 4.5\lambda$, $\gamma = 0.08\,\mathrm{rad}$, $a_{\max} = 2.0$, $k_{z,\mathrm{tail}} = 0.20k$, $k_{y,\mathrm{tail}} = 0.20\,\mathrm{Re}[\kappa]$, $C_z = 10.0$, $C_y = 15.0$.

These parameters are chosen such that the relative error obtained in the evaluation of $g(\mathbf{r}, \mathbf{r}')$ in the spectral domain as discussed in Ref. 22 is less than 0.5%.

Numerical results are presented in terms of the normalized incoherent radar cross section (RCS) $\sigma^i_{\alpha\beta}(\theta_s, \theta_i)$ in the plane of incidence, defined for a scattered wave in α polarization and an incident wave in β polarization as

$$\sigma^i_{\alpha\beta}(\theta_s, \theta_i) = \lim_{r \to \infty} 4\pi r^2 \langle |\widetilde{\mathbf{E}^s_{\alpha\beta}} - \langle \widetilde{\mathbf{E}^s_{\alpha\beta}} \rangle|^2 \rangle \cos\theta_i, \quad (2)$$

where $\widetilde{\mathbf{E}^s_{\alpha\beta}}$ is defined as

$$\widetilde{\mathbf{E}^s_{\alpha\beta}} = \frac{\mathbf{E}^s_{\alpha\beta}}{\left(2\eta \int_S \mathbf{S}^i_\beta \cdot \hat{n}_{\mathrm{in}} \mathrm{d}s \right)^{1/2}}, \quad (3)$$

$\mathbf{E}^s_{\alpha\beta}$ is the α-polarized scattered field of the β-polarized incident wave, θ_i and θ_s refer to the incident and the scattered polar angles, respectively (see Fig. 1), η is the free-space intrinsic impedance, $\hat{n}_{\mathrm{in}}$ is a unit normal vector pointing into the rough surface from the free-space region, $\mathbf{S}^i_\beta$ is the time-averaged Poynting vector of the β-polarized incident wave, S is the 2-D rough-surface profile of interest, and $\langle\ \rangle$ indicates an ensemble average over realizations of the surface stochastic process.

3. NUMERICAL RESULTS AND DISCUSSION

In this section, variations in the characteristics of backscattering enhancement with incident angle, surface material, polarization, and surface statistics are discussed.

A. Effects of Incident Angle

For convenience in discussion, we define the angular regions $-90° \leqslant \theta_s \leqslant 0°$ and $0° \leqslant \theta_s \leqslant 90°$ to be the forward and the backward angular regions, respectively. Figures 2 and 3 compare the co-polarized and cross-polarized normalized incoherent bistatic RCS with various incident angles for the case of PEC Gaussian surfaces with an isotropic Gaussian spectrum $h/\lambda = \sigma_s = 1.0$ for $0° \leqslant \theta_i \leqslant 40°$ and $60° \leqslant \theta_i \leqslant 70°$, respectively. While some residual variations in bistatic scattering patterns are observed as a result of the finite number of realizations employed in the Monte Carlo study, basic trends of the data remain discernible. It can be seen from these plots that the overall level of the normalized incoherent bistatic RCS tends to decrease as the incident angle θ_i increases from 0° to 70° for both co-polarization and cross polarization, as should be expected. Note that backscattering enhancement exists only for small θ_i from 0° to 40°; i.e., no well-defined backscattering peak exists for the 60° and 70° angles. However, the co-polarized scattered energy tends to be distributed largely in the backward angular region for all θ_i of interest, even with relatively large θ_i. It can also be observed that there are some differences between the HH and the VV scattering patterns. For example, VV polarization exhibits a secondary peak at the specular direction for $\theta_i = 20°$, but no such peak exists for HH polarization, as was also observed

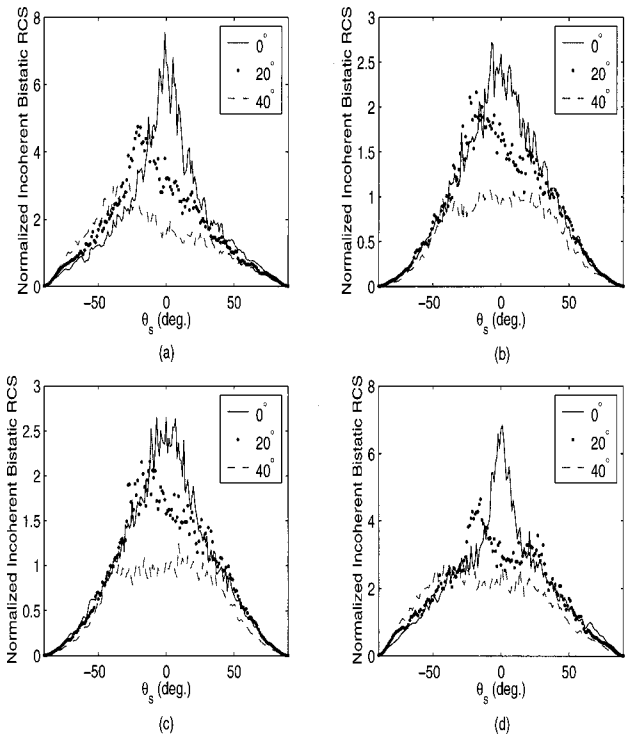

Fig. 2. Comparison of Monte Carlo 2-D FB–NSA results (150 realizations) with various incident angles ($0° \leqslant \theta_i \leqslant 40°$) for PEC Gaussian surfaces with an isotropic Gaussian spectrum $h/\lambda = \sigma_s = 1.0$ and $l_x = l_y = \sqrt{2}\lambda$: (a) HH polarization, (b) VH polarization, (c) HV polarization, (d) VV polarization.

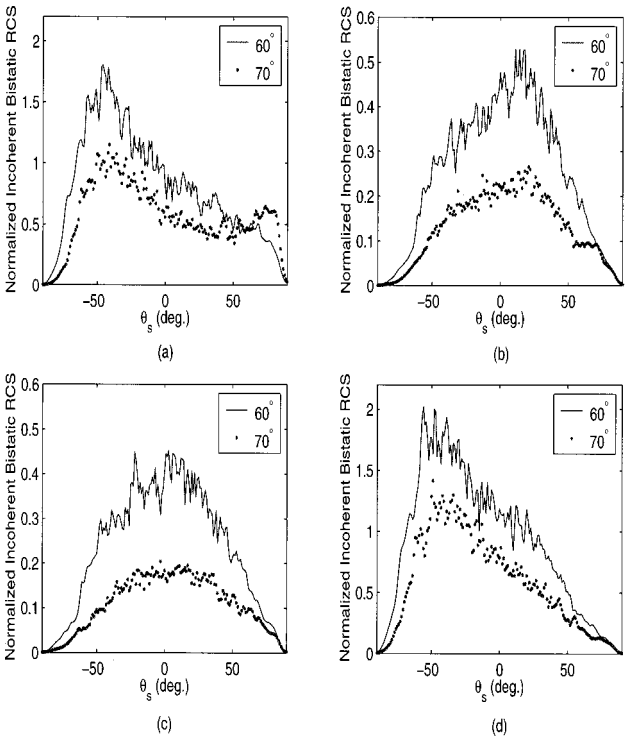

Fig. 3. Comparison of Monte Carlo 2-D FB–NSA results (150 realizations) with various incident angles ($60° \leqslant \theta_i \leqslant 70°$) for PEC Gaussian surfaces with an isotropic Gaussian spectrum $h/\lambda = \sigma_s = 1.0$ and $l_x = l_y = \sqrt{2}\lambda$: (a) HH polarization, (b) VH polarization, (c) HV polarization, (d) VV polarization.

previously.[11] For a higher angle of incidence $\theta_i = 70°$, HH polarization exhibits a secondary peak in the neighborhood of the specular direction, whereas VV polarization does not. VH scattering patterns are similar to those in HV polarization, and, as θ_i increases, the scattering patterns tend to broaden and become more nearly uniform.

Figures 4 and 5 repeat the computations of Figs. 2 and 3 with IBC rough surfaces with $\epsilon_{r1} = 10.0 + i10.0$ for $0° \leqslant \theta_i \leqslant 40°$ and $60° \leqslant \theta_i \leqslant 70°$, respectively. From Figs. 2–5 it is observed that as the magnitude of ϵ_{r1} ($|\epsilon_{r1}|$) decreases, the overall level of the bistatic RCS decreases noticeably. Cross-polarized scattering patterns reduce in amplitude but are otherwise similar to those in the PEC case. As in the PEC case, co-polarized scattered energy with IBC surfaces is distributed primarily in the backward angular region for all incident angles of interest. However, some co-polarized scattering characteristics of PEC and IBC surfaces are different. In Fig. 4 the VV backscattering peak for $\theta_i = 40°$ exceeds the VV backscattering peak for $\theta_i = 0°$, 20°. This is an unusual phenomenon, which was observed in 1-D surface results as well.[22] As $|\epsilon_{r1}|$ decreases and θ_i increases, both HH and VV polarizations tend to exhibit more scattered energy near the specular direction.

Figures 6 and 7 illustrate results for PEC surfaces with $h/\lambda = \sigma_s = 0.5$. Comparing Figs. 6 and 7 with Figs. 2 and 3, we find that the overall bistatic RCS level decreases noticeably as σ_s decreases from 1.0 to 0.5. In Figs. 6 and 7 the backscattering peak exists for $\theta_i = 0°$,

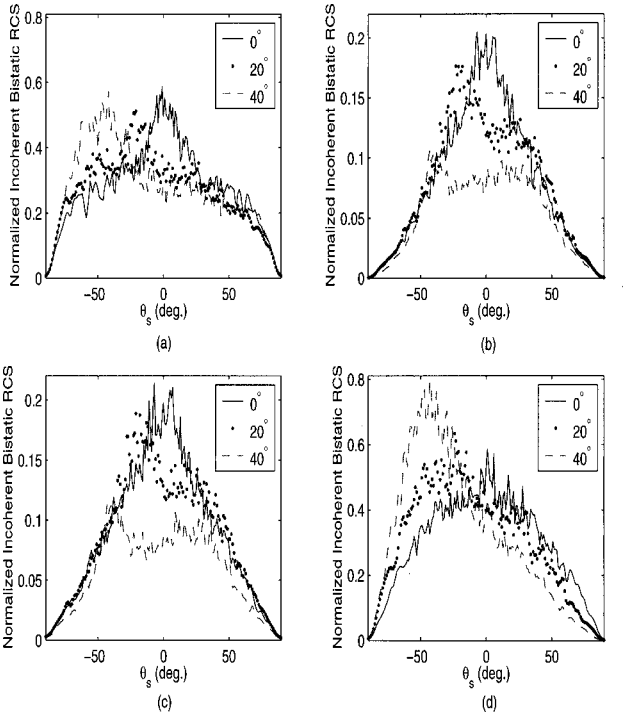

Fig. 4. Comparison of Monte Carlo 2-D FB–NSA results (150 realizations) with various incident angles ($0° \leqslant \theta_i \leqslant 40°$) for IBC Gaussian surfaces with relative permittivity $\epsilon_{r1} = 10.0 + i10.0$ and an isotropic Gaussian spectrum $h/\lambda = \sigma_s = 1.0$ and $l_x = l_y = \sqrt{2}\lambda$: (a) HH polarization, (b) VH polarization, (c) HV polarization, (d) VV polarization.

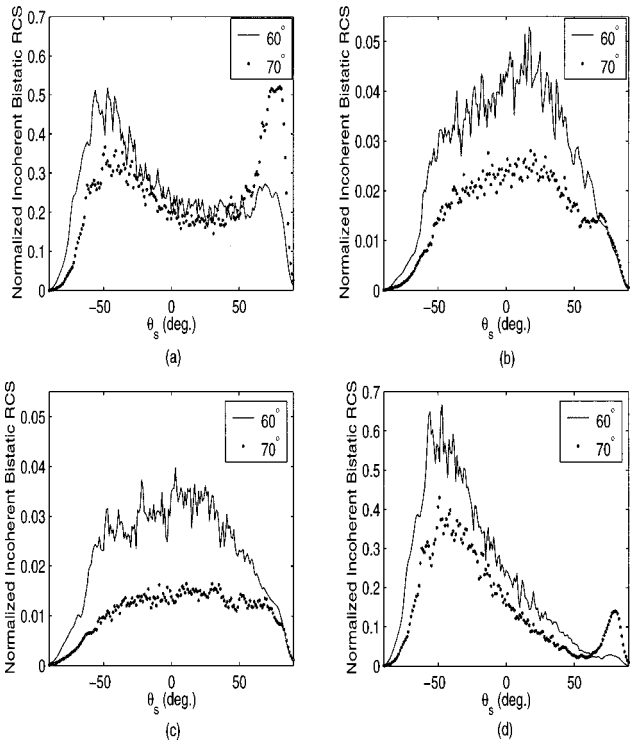

Fig. 5. Comparison of Monte-Carlo 2-D FB–NSA results (150 realizations) with various incident angles ($60° \leqslant \theta_i \leqslant 70°$) for IBC Gaussian surfaces with relative permittivity $\epsilon_{r1} = 10.0 + i10.0$ and an isotropic Gaussian spectrum $h/\lambda = \sigma_s = 1.0$ and $l_x = l_y = \sqrt{2}\lambda$: (a) HH polarization, (b) VH polarization, (c) HV polarization, (d) VV polarization.

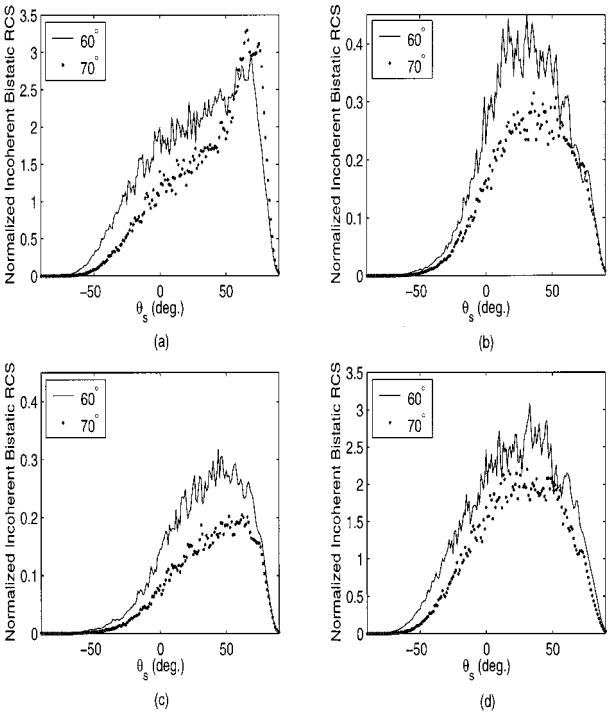

Fig. 7. Comparison of Monte Carlo 2-D FB–NSA results (150 realizations) with various incident angles ($60° \leqslant \theta_i \leqslant 70°$) for PEC Gaussian surfaces with an isotropic Gaussian spectrum $h/\lambda = \sigma_s = 0.5$ and $l_x = l_y = \sqrt{2}\lambda$: (a) HH polarization, (b) VH polarization, (c) HV polarization, (d) VV polarization.

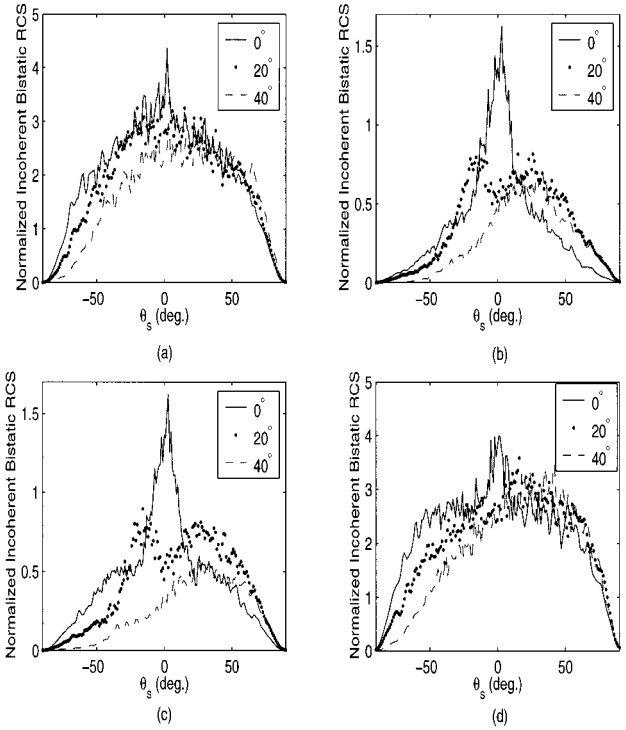

Fig. 6. Comparison of Monte Carlo 2-D FB–NSA results (150 realizations) with various incident angles ($0° \leqslant \theta_i \leqslant 40°$) for PEC Gaussian surfaces with an isotropic Gaussian spectrum $h/\lambda = \sigma_s = 0.5$ and $l_x = l_y = \sqrt{2}\lambda$: (a) HH polarization, (b) VH polarization, (c) HV polarization, (d) VV polarization.

and 20° only. Thus it can be concluded that higher surface slopes contribute to the backscattering enhancement. Cross-polarized results exhibit backscattering enhancement more clearly than co-polarized results for this case since multiple-scattering effects are not obscured by first-order scattering for cross polarization. Scattering characteristics of the HH and the VV polarizations are again different, with HH polarization exhibiting more scattered energy near the specular direction than VV polarization as θ_i increases. Unlike for $\sigma_s = 1.0$, the co-polarized scattered energy is distributed largely in the backward angular region only for small θ_i. As θ_i increases toward grazing incidence, both co-polarized and cross-polarized scattered energies tend to migrate from the backward angular region to the forward angular region.

In summary, as the incident angle increases, the overall bistatic RCS level tends to decrease, and backscattering enhancement does not exist for larger incident angles. According to the Rayleigh criterion,[26] rough surfaces appear to be smoother as the incident angle increases, which possibly explains the disappearance of the backscattering enhancement at higher angles of incidence. However, numerical results illustrate that increasing surface slopes and surface roughness can contribute to backscattering enhancement. Cross polarization exhibits backscattering enhancement more clearly than does co-polarization, and HH polarization exhibits more scattered energy near the specular direction than VV polarization as θ_i increases.

B. Effects of Surface Material

Figures 8, 9, and 10 illustrate results for various surface materials with $h/\lambda = \sigma_s = 1.0$ for $\theta_i = 0°$, 40°, 70°, respectively. Note that the vertical line in each plot of these figures corresponds to the backscattering direction. For convenience of comparison, the normalized incoherent bistatic RCS for the IBC surfaces is scaled such that its maximum is equal to the maximum for the PEC surfaces, and the scaling factor is shown in parentheses appended to the value of ϵ_{r1} in each plot. From these figures it can be seen that the overall bistatic RCS level increases as the surface material becomes denser (i.e., increasing $|\epsilon_{r1}|$) because of the stronger reflections of scattered EM fields for the denser surface material.[7] In addition, for a fixed incident angle the scattering patterns for each surface material follow similar trends in both co-polarization and cross polarization. Figures 8 and 9 illustrate that the backscattering peak clearly exists for all four polarizations, and the VH and HV scattering patterns look very similar. For $\theta_i = 0°$, the co-polarized scattering pattern for the denser surfaces tends to be more concentrated in the backscattering direction. For $\theta_i = 70°$, a peak does not exist in the backscattering direction, although most of the scattered energy is still distributed largely in the backward angular region. HH polarization again exhibits more scattered energy near the specular direction than VV polarization for all surface materials of interest, and the peak in the forward angular region for HH polarization can exceed the peak in the backward angular region as $|\epsilon_{r1}|$ decreases. For cross polarization at $\theta_i = 70°$, the peak tends to exist in the for-

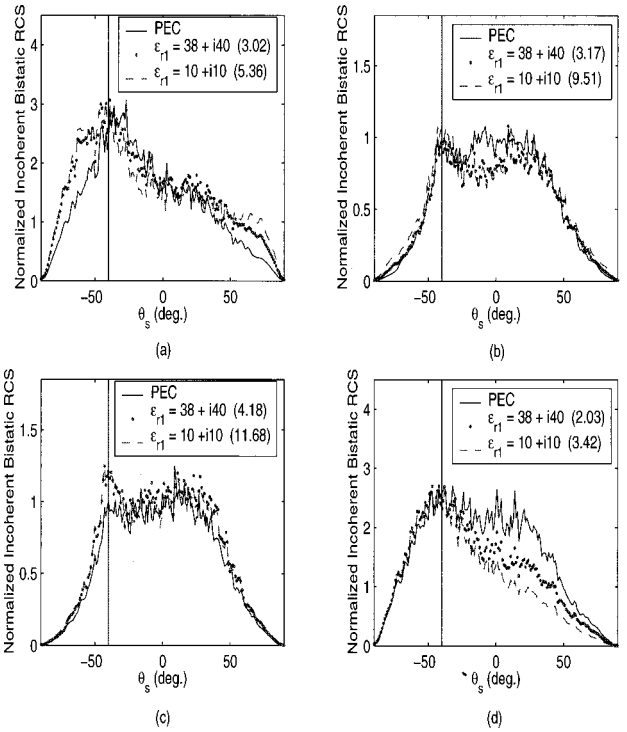

Fig. 9. Comparison of Monte Carlo 2-D FB–NSA results (150 realizations) with various surface materials at $\theta_i = 40°$ for Gaussian surfaces with an isotropic Gaussian spectrum $h/\lambda = \sigma_s = 1.0$ and $l_x = l_y = \sqrt{2}\lambda$: (a) HH polarization, (b) VH polarization, (c) HV polarization, (d) VV polarization.

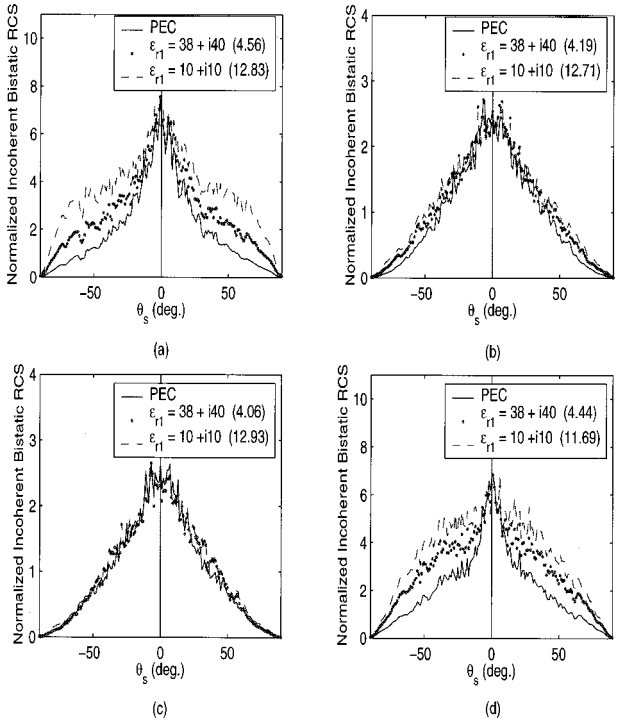

Fig. 8. Comparison of Monte Carlo 2-D FB–NSA results (150 realizations) with various surface materials at $\theta_i = 0°$ for Gaussian surfaces with an isotropic Gaussian spectrum $h/\lambda = \sigma_s = 1.0$ and $l_x = l_y = \sqrt{2}\lambda$: (a) HH polarization, (b) VH polarization, (c) HV polarization, (d) VV polarization.

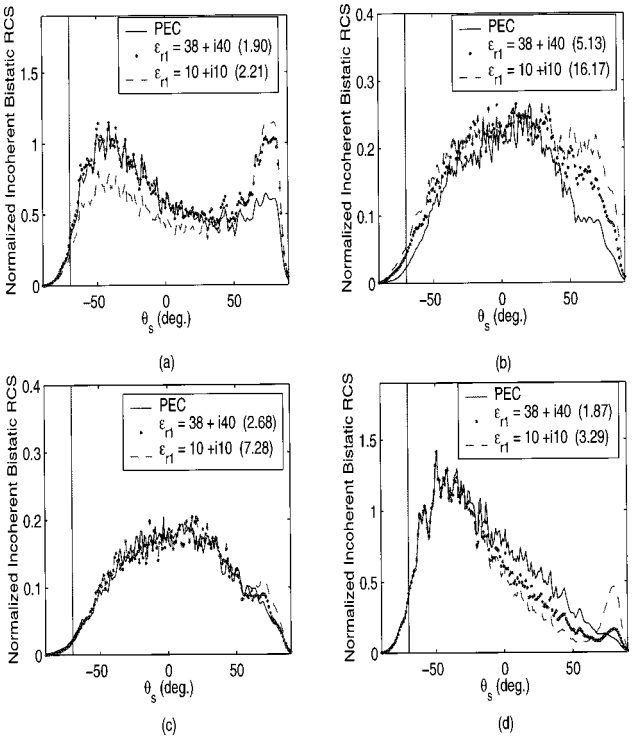

Fig. 10. Comparison of Monte Carlo 2-D FB–NSA results (150 realizations) with various surface materials at $\theta_i = 70°$ for Gaussian surfaces with an isotropic Gaussian spectrum $h/\lambda = \sigma_s = 1.0$ and $l_x = l_y = \sqrt{2}\lambda$: (a) HH polarization, (b) VH polarization, (c) HV polarization, (d) VV polarization.

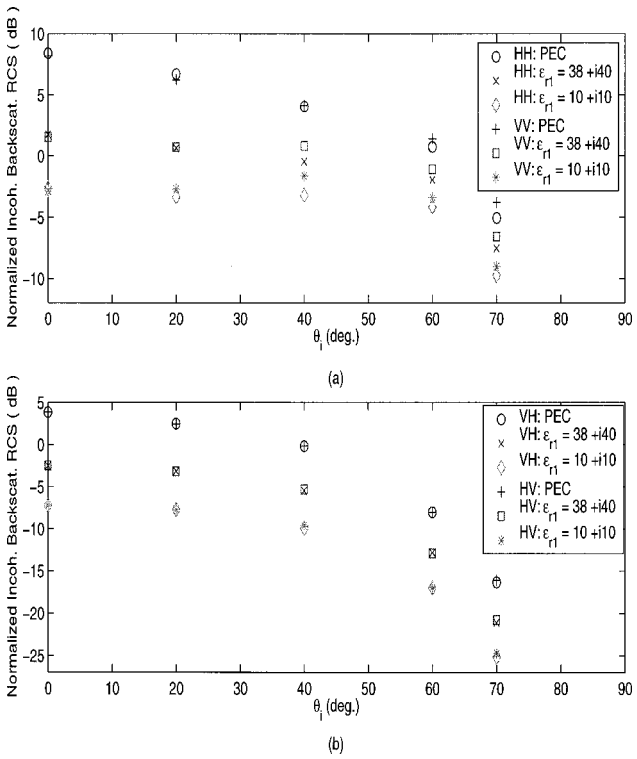

Fig. 11. Comparison of the normalized incoherent backscattering RCS (in decibels) computed by the Monte Carlo 2-D FB–NSA method (150 realizations) averaged over the three consecutive angles in 1-deg steps (including the backscattering angle) nearby the backscattering direction of interest with various surface materials for Gaussian surfaces with an isotropic Gaussian spectrum $h/\lambda = \sigma_s = 1.0$ and $l_x = l_y = \sqrt{2}\lambda$: (a) co-polarization, (b) cross polarization.

ward angular region instead of in the backward angular region, and VH and HV polarizations are slightly different.

Figure 11 shows a comparison of the normalized incoherent backscattering RCS (in decibels) with various surface materials for $h/\lambda = \sigma_s = 1.0$. The backscattering RCS results are averaged (magnitudes of backscattered fields) over three consecutive bistatic angles in 1-deg steps (including the backscattering angle). From the plots, it is observed that the normalized co-polarized and cross-polarized incoherent backscattering radar cross sections decrease as $|\epsilon_{r1}|$ decreases. Also note that the VH and HV backscattering patterns for each surface material are almost identical as a result of reciprocity, as expected. However, the HH and VV backscattering patterns are slightly different for each surface material.

C. Effects of Surface Statistics

Figures 12 and 13 illustrate PEC surface results for various rms surface slopes $\sigma_s = 0.5, 0.707, 1.0$ for $\theta_i = 20°$ and 70°, respectively. Figure 12 shows that all surface statistics of interest exhibit backscattering enhancement at $\theta_s = -20°$, as marked by the vertical lines, and cross polarization exhibits the backscattering enhancement more clearly than does co-polarization, as expected. We also note that, as σ_s increases, the backscattering peak tends to increase. In addition, the VH and HV scattering patterns are similar for all surface statistics, but the HH

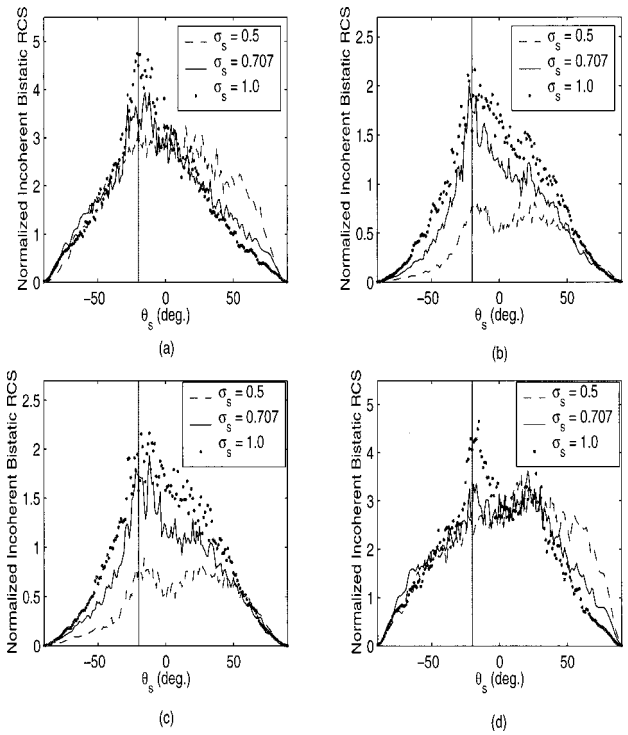

Fig. 12. Comparison of Monte Carlo 2-D FB–NSA results (150 realizations) with various rms surface slopes at $\theta_i = 20°$ for PEC Gaussian surfaces with an isotropic Gaussian spectrum $l_x = l_y = \sqrt{2}\lambda$: (a) HH polarization, (b) VH polarization, (c) HV polarization, (d) VV polarization.

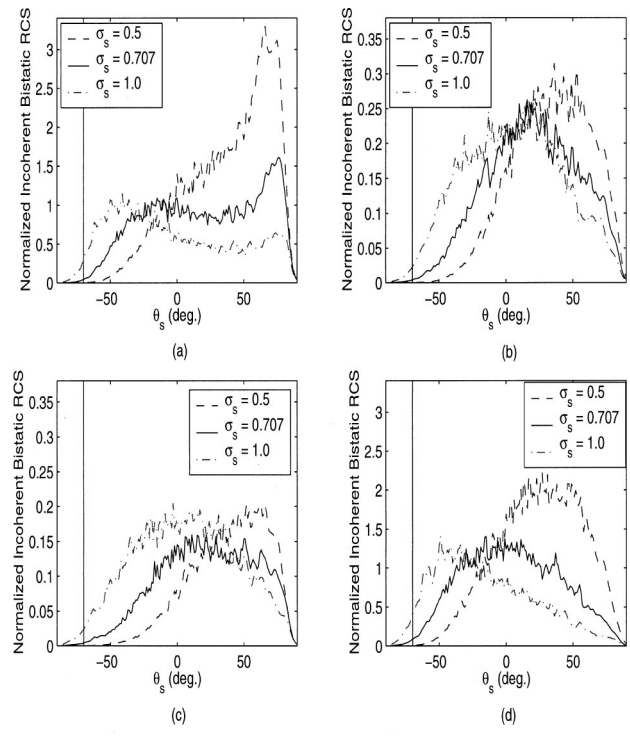

Fig. 13. Comparison of Monte Carlo 2-D FB–NSA results (150 realizations) with various rms surface slopes at $\theta_i = 70°$ for PEC Gaussian surfaces with an isotropic Gaussian spectrum $l_x = l_y = \sqrt{2}\lambda$: (a) HH polarization, (b) VH polarization, (c) HV polarization, (d) VV polarization.

and VV scattering patterns are different. As σ_s decreases (i.e., surfaces become smoother), the scattered energy in the forward angular region tends to increase for both co-polarization and cross polarization. In Fig. 13, no surface statistics exhibit a well-defined backscattering peak at $\theta_s = -70°$, as marked by the vertical lines, even for cross polarization with the highest surface slope, $\sigma_s = 1.0$. As σ_s decreases, the scattering patterns tend to migrate from the backward angular region to the forward angular region for both co-polarization and cross polarization. In addition, the HH and VV polarizations exhibit distinct scattering patterns for all surface statistics of interest. For cross polarization, the overall VH bistatic RCS level exceeds the overall HV bistatic RCS level for all σ_s.

Figure 14 plots normalized incoherent backscattering radar cross sections (in decibels) with various rms surface slopes $\sigma_s = 0.1, 0.5, 1.0$ for PEC Gaussian surfaces. For the relatively smooth surfaces with $\sigma_s = 0.1$, the second-order small-slope approximation (SSA) is employed to compute the backscattering RCS because of efficiency for small-slope surfaces. Although analytical ensemble-average results can be efficiently computed for the first-order SSA, obtaining ensemble averages for the higher-order terms that are required for predicting surface cross-polarized backscattering rapidly becomes impractical. Thus the second-order SSA employed in this study is applied in a Monte Carlo simulation to obtain ensemble-average SSA predictions and requires an $\mathcal{O}(N_{\text{tot}} \log_2 N_{\text{tot}})$ computation. For the SSA computation, surface sizes of 128λ by 32λ sampled with eight unknowns per EM wavelength are employed, and 100 surface realizations are employed to obtain accurate incoherent backscattering RCS results. From the plots we can observe that the co-polarized and cross-polarized backscattering radar cross sections tend to increase at oblique observation angles as σ_s increases, and variations with θ_i for the rougher surfaces are typically slower than those for smoother surfaces ($\sigma_s = 0.1$) in both co-polarization and cross polarization. In addition, the HH and VV backscattering patterns are different, although they follow similar trends. Furthermore, it is found that the HH/VV polarization ratio tends to decrease as θ_i increases and/or σ_s decreases, with smoother surface results decreasing more rapidly with θ_i.

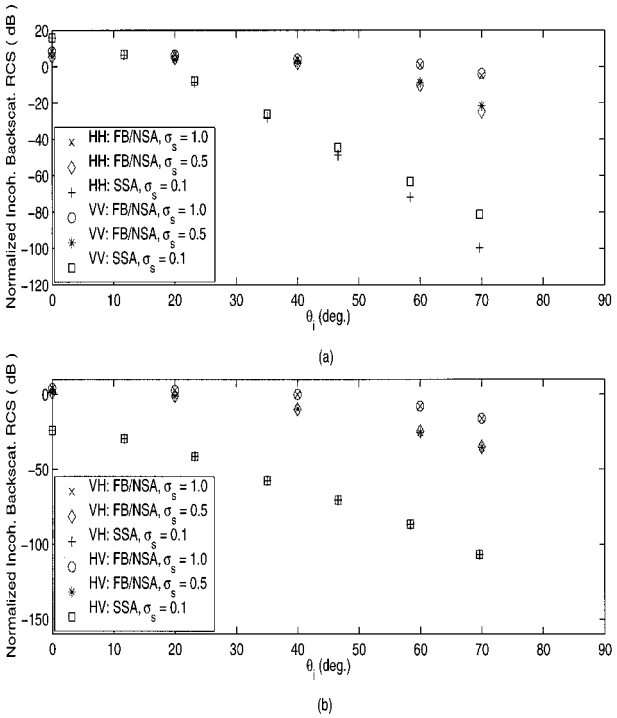

Fig. 14. Comparison of the normalized incoherent backscattering RCS (in decibels) computed by the Monte Carlo 2-D FB–NSA method (150 realizations) averaged over the three consecutive angles in 1-deg steps (including the backscattering angle) nearby the backscattering direction of interest and the Monte Carlo SSA (up to second order and for 100 realizations) with various rms surface slopes for PEC Gaussian surfaces with an isotropic Gaussian spectrum $l_x = l_y = \sqrt{2}\lambda$: (a) co-polarization, (b) cross polarization.

4. SUMMARY AND CONCLUSIONS

Results of this study show that backscattering enhancement depends strongly on incident angle, surface material, polarization, and surface statistics as follows:

- As incident angle increases, smaller backscattering enhancement effects are observed, even when the very rough and large-slope surfaces are considered.
- The normalized incoherent backscattering RCS tends to increase as surfaces become denser.
- Cross polarization exhibits backscattering enhancement more clearly than does co-polarization because of the absence of the cross-polarized first-order scattering.
- The scattering characteristics of HH and VV polarizations are different, with HH polarization typically exhibiting more scattered energy near the specular direction than does VV polarization as θ_i increases.
- The backscattering peak, the backscattering RCS, and the HH/VV polarization ratio tend to increase as the surface roughness and the surface slope increase. In addition, variations of the backscattering RCS and the HH/VV polarization ratio with incident angle are slower for the rougher surfaces.

Although all these conclusions are in agreement with typical expectations of rough-surface scattering theory, the true merit of the results illustrated here is their ability to be used in comparisons with new theories of backscattering enhancement.

ACKNOWLEDGMENTS

This work was sponsored by U.S. Office of Naval Research contracts N00014-97-1-0541 and N00014-00-1-0399 and National Science Foundation project ECS-9701678. Use of the IBM SP system at the Maui High Performance Computing Center is acknowledged; it was sponsored by the U.S. Air Force Research Laboratory, Air Force Materiel Command under cooperative agreement F29601-93-2-0001. Opinions, interpretations, conclusions, and recommendations are those of the authors and are not necessarily endorsed by the U.S. Air Force, the U.S. Air Force Research Laboratory, or the U.S. government. Use of the CRAY T3E computer at the Ohio Supercomputing Center is also acknowledged.

Corresponding author Joel Johnson's e-mail address is johnson@ee.eng.ohio-state.edu.

REFERENCES

1. A. Ishimaru, "Experimental and theoretical studies on enhanced backscattering from scatterers and rough surfaces," in *Scattering in Volumes and Surfaces*, M. Nieto-Vesperinas and J. C. Dainty, eds. (North-Holland, Amsterdam, 1990), pp. 1–15.
2. A. Ishimaru, "Backscattering enhancement: from radar cross sections to electron and light localizations to rough-surface scattering," IEEE Antennas Propag. Mag. **33**, 7–11 (1991).
3. K. A. O'Donnell and E. R. Mendez, "Experimental study of scattering from random rough surfaces," J. Opt. Soc. Am. A **4**, 1194–1205 (1987).
4. M. J. Kim, J. Dainty, A. Friberg, and A. Sant, "Experimental study of enhanced backscattering from one- and two-dimensional random rough surfaces," J. Opt. Soc. Am. A **7**, 569–577 (1990).
5. A. A. Maradudin, J. Q. Lu, P. Tran, R. F. Wallis, V. Celli, Z. H. Gu, A. R. McGurn, E. R. Mendez, T. Michel, M. Nieto-Vesperinas, J. C. Dainty, and A. J. Sant, "Enhanced backscattering from one- and two-dimensional random surfaces," Rev. Mex. Fis. **38**, 343–397 (1992).
6. P. Phu, A. Ishimaru, and Y. Kuga, "Co-polarized and cross-polarized enhanced backscattering from two-dimensional very rough surfaces at millimeter wave frequencies," Radio Sci. **29**, 1275–1291 (1994).
7. A. Ishimaru, C. Le, Y. Kuga, L. A. Sengers, and T. K. Chan, "Polarimetric scattering theory for high slope rough surfaces," Prog. Electromagn. Res. **14**, 1–36 (1996).
8. C. Hsieh and A. K. Fung, "Application of an extended IEM to multiple surface scattering and backscatter enhancement," J. Electromagn. Waves Appl. **13**, 121–135 (1999).
9. E. Bahar and M. El-Shenawee, "Enhanced backscatter from one dimensional random rough surfaces—stationary phase approximations to full wave solutions," J. Opt. Soc. Am. A **12**, 151–161 (1995).
10. P. Tran, V. Celli, and A. A. Maradudin, "Electromagnetic scattering from a two-dimensional randomly rough, perfectly conducting surface: iterative methods," J. Opt. Soc. Am. A **11**, 1686–1689 (1994).
11. J. T. Johnson, L. Tsang, R. T. Shin, K. Pak, C. H. Chan, A. Ishimaru, and Y. Kuga, "Backscattering enhancement of electromagnetic waves from two-dimensional perfectly conducting random rough surfaces: a comparison of Monte Carlo simulations with experimental data," IEEE Trans. Antennas Propag. **44**, 748–756 (1996).
12. K. Pak, L. Tsang, C. H. Chan, and J. T. Johnson, "Backscattering enhancement of electromagnetic waves from two-dimensional perfectly conducting random rough surfaces based on Monte Carlo simulations," J. Opt. Soc. Am. A **12**, 2491–2499 (1995).
13. K. Pak, L. Tsang, and J. T. Johnson, "Numerical simulations and backscattering enhancement of electromagnetic waves from two-dimensional dielectric random rough surfaces with the sparse-matrix canonical grid method," J. Opt. Soc. Am. A **14**, 1515–1529 (1997).
14. R. L. Wagner, J. M. Song, and W. C. Chew, "Monte Carlo simulation of electromagnetic scattering from two-dimensional random rough surfaces," IEEE Trans. Antennas Propag. **45**, 235–245 (1997).
15. V. Jandhyala, E. Michielssen, S. Balasubramaniam, and W. C. Chew, "A combined steepest descent–fast multipole algorithm for the fast analysis of three-dimensional scattering by rough surfaces," IEE Trans. Geosci. Remote Sens. **36**, 738–748 (1998).
16. R. F. Harrington, *Field Computation by Moment Methods* (Krieger, Malarbar, Fla., 1982).
17. H.-T. Chou and J. T. Johnson, "A novel acceleration algorithm for the computation of scattering from rough surfaces with the forward–backward method," Radio Sci. **33**, 1277–1287 (1998).
18. H.-T. Chou and J. T. Johnson, "Formulation of forward–backward method using novel spectral acceleration for the modeling of scattering from impedance rough surfaces," IEEE Trans. Geosci. Remote Sens. **38**, 605–607 (2000).
19. D. Torrungrueng, H.-T. Chou, and J. T. Johnson, "A novel acceleration algorithm for the computation of scattering from two-dimensional large-scale perfectly conducting random rough surfaces with the forward-backward method," IEEE Trans. Geosci. Remote Sens. **38**, 1656–1668 (2000).
20. D. Torrungrueng, J. T. Johnson, and H.-T. Chou, "Some issues related to the novel spectral acceleration (NSA) method for the fast computation of radiation/scattering from one-dimensional extremely large-scale quasi-planar structures," manuscript available from the authors.
21. D. Torrungrueng and J. T. Johnson, "The forward–backward method with a novel acceleration algorithm (FB/NSA) for the computation of scattering from two-dimensional large-scale impedance random rough surfaces," Microwave Opt. Technol. Lett. **29**, 232–236 (2001).
22. D. Torrungrueng, "Applications of the novel spectral acceleration (NSA) algorithm for the computation of scattering from rough surfaces," Ph.D. dissertation (Ohio State University, Columbus, Ohio, 2000).
23. J. T. Johnson, R. T. Shin, J. A. Kong, L. Tsang, and K. Pak, "A numerical study of ocean polarimetric thermal emission," IEEE Trans. Geosci. Remote Sens. **37**, 8–20 (1999).
24. T. B. A. Senior, "Impedance boundary conditions for imperfectly conducting surface," Appl. Sci. Res. Sect. B **8**, 418–436 (1960).
25. A. A. Maradudin, "The impedance boundary condition at a two-dimensional rough metal surface," Opt. Commun. **116**, 452–467 (1995).
26. P. Beckmann and A. Spizzichino, *The Scattering of Electromagnetic Waves from Rough Surfaces* (Pergamon, New York, 1963).
27. A. G. Voronovich, *Wave Scattering from Rough Surfaces* (Springer-Verlag, Berlin, 1994).
28. S. T. McDaniel, "Acoustic and radar scattering from directional seas," Waves Random Media **9**, 537–549 (1999).